JOURNAL OF SOLID STATE CHEMISTRY 116, 118–130 (1995)

Synthesis, Crystal Structure, and Unusual Magnetic Properties of $InMnO_3$

J. E. Greedan,[1] M. Bieringer, and J. F. Britten

Institute for Materials Research, McMaster University, Hamilton, Ontario, Canada L8S 4M1

and

D. M. Giaquinta and H.-C. zur Loye[1]

Department of Chemistry, Massachusetts Institute of Technology, Cambridge, Massachusetts 02139

Received June 15, 1994; in revised form September 12, 1994; accepted September 15, 1994

Polycrystalline samples of $InMnO_3$, prepared by decomposition of nitrates, were found to be isostructural with $LuMnO_3$ rather than $YAlO_3$ as was the case for flux-grown $InMnO_3$ single crystals. The structure was refined in $P6_3cm$ from powder neutron data with $a = 5.8758(4)$ Å and $c = 11.4715(8)$ Å at 293 K. Single crystals of $ScMnO_3$ were grown from a PbF_2 flux. The structure was refined from single crystal X-ray data also in $P6_3cm$ with $a = 5.8286(6)$ Å and $c = 11.1738(9)$ Å. Magnetic susceptibility data for $InMnO_3$ show subtle anomalies near 120 and 40 K and a weak maximum at 15 K for applied fields <0.05 T. Neutron diffraction data reveal a complex structure with two distinct classes of reflections. From 295 to 5 K, a broad (100) reflection is seen which is well described by a Warren-type lineshape and which is assigned to two-dimensional in-plane Mn–Mn spin correlations. Below 120 K, reflections indexed as (h 0 $n/2$) and (h l $n/2$) appear which exhibit an unusual temperature dependence featuring intensity maxima near 60–70 K and which are significantly broader than the resolution limit at all temperatures. These are assigned to correlations between spin-coupled Mn layers, also of short range. The absence of long-range order in $InMnO_3$ is contrasted with the well-established order in isostructural $ScMnO_3$ and $LnMnO_3$. It is argued that the differences can be rationalized in terms of an anomalously long c-axis for $InMnO_3$ which leads to a weakening of key interlayer superexchange pathways necessary for the realization of long-range order. This situation is also discussed in terms of recent mean-field theory for layered antiferromagnets.

INTRODUCTION

Mixed oxides of composition ABO_3 have been the object of more studies than perhaps any class of solid materials. Included in this vast family are oxides with well-known structure types such as corundum or ilmenite, bixbyite or C–M_2O_3, and, of course, the myriad perovskite-related structures. The discovery of a new ABO_3 material such as $InMnO_3$ (1) is thus a fairly rare phenomenon. The only other reported ternary oxide involving these metals is the defect spinel $In_{2-x}Mn_{1+x}O_4$, which forms if a mixture of In_2O_3 and Mn_2O_3 is heated in air (2).

The crystal structure of $InMnO_3$, determined from Bi_2O_3-flux-grown single crystals, is of the $YAlO_3$-type, described in $P6_3/mmc$ (1). This is an interesting result. The effective ionic radius of In(III) (six-fold), 0.800 Å, is intermediate between Lu (III) 0.861 Å, and Sc(III) 0.745 Å (3). Both $LuMnO_3$ and $ScMnO_3$ are reported to have a hexagonal structure which is a slightly distorted variant of $YAlO_3$ (4, 5). The $LuMnO_3$ structure type is described in $P6_3cm$ and is a supercell of the $YAlO_3$ type with $a = 3^{1/2}a$ of the latter but retaining the same c-axis periodicity. No detailed structure of $ScMnO_3$ has been reported, but the cell constants suggest that it is isostructural with $LuMnO_3$ (5).

In the $LuMnO_3$ structure the large cation has sevenfold coordination, while Mn(III) has unusual fivefold, trigonal bipyramidal coordination. The Mn(III) ions are arranged in hexagonal layers, separated by Lu–O layers, stacked in an ABAB or hexagonal close-packed manner. Such ABAB stacking of magnetic ion layers is fairly rare, and under the condition of nearest neighbor intra- and interplanar antiferromagnetic interactions it can give rise to frustrated magnetic behavior in three dimensions, as discussed recently by Reimers and Dahn (6). $YMnO_3$ and $LuMnO_3$ show so-called triangular magnetic structures in which the spins, $S = 2$ for Mn^{3+}, within a layer are oriented at 120°, giving evidence for this frustration effect (7, 8).

In this study, we report the preparation and crystal

[1] To whom correspondence should be addressed.

0022-4596/95 $6.00

structure of polycrystalline $InMnO_3$ obtained by a different synthetic route than the crystals in (1) and we examine the magnetic properties of this material using bulk magnetic and neutron diffraction techniques. The structure and magnetic properties of $InMnO_3$ are compared to those of $LuMnO_3$ and $ScMnO_3$. The detailed structure of $ScMnO_3$ is also reported for the first time.

EXPERIMENTAL

Sample Preparation

$InMnO_3$. Polycrystalline samples of $InMnO_3$ were prepared using a nitrate decomposition technique (9). Using a 10-mmole scale, a slight excess of $In(OH)_3$ (Johnson Matthey, 99.999%) was dissolved in 100 ml of concentrated HNO_3 with Mn(II) acetate tetrahydrate (Johnson Matthey, 99.999%) in a 400-ml beaker. An excess of indium hydroxide (6 mole%) was necessary to compensate for indium lost during the synthesis and to ensure a single phase product of $InMnO_3$. If stoichiometric amounts of indium and manganese were used in the preparation of the precursor, the presence of manganese oxide was seen by powder X-ray diffraction. Since the sample was intended for magnetic measurements, a larger excess of indium than normal was used to ensure the absence of any magnetic manganese impurities. This larger excess, however, led to a small amount of nonmagnetic In_2O_3 impurity in the final product.

A beaker of the nitric acid solution was heated on a hotplate set to low heat with stirring until the solution became colorless. The temperature of the hotplate was then increased to allow slow evaporation of the liquid. When less than 10 ml of liquid remained, the beaker was removed from the hotplate, allowing the remaining liquid to solidify into a clear paste. The beaker was then placed into a box furnace and heated to 550°C for 12 hr, during which time the clear precursor became a low-density, black solid. The black solid was ground in an agate mortar and sealed in an evacuated quartz tube. The quartz tube was heated to 1000°C for 48 hr resulting in a black product that consisted of small, hexagon-shaped single crystallites visible under a microscope. It should be noted that the quartz tubes contained excess pressure that was noticeable as an explosive popping when the tube was opened.

TABLE 1
Crystal Data for $ScMnO_3$

Color, habit	Black, triangular plate
Crystal size (mm)	0.69 × 0.69 × 0.003
Crystal system	Hexagonal
Space group	$P6_3cm$
Unit cell dimensions (Å)	a = 5.8286(6)
	c = 11.1738(9)
Volume (Å)	328.80
Z	6
Density (calc) (Mg/m^3)	4.482
Formula weight (g/mole)	147.90
Absorption coefficient	8.54 mm^{-1}
$F(000)$	420.00

TABLE 2
Conditions for Single Crystal Data Collection and Refinement on $ScMnO_3$

Diffractometer used	Siemens P4
Radiation	Mo$K\alpha$ (λ = 0.71073 Å), rotating anode
Temperature (K)	293(2)
Monochromator	Highly oriented graphite crystal
Scan type	$2\theta - \theta$
Scan speed	Variable; 1.50 to 14.00°/min.
Scan range (ω)	1.00° plus $K\alpha$-separation
Background measurement	Stationary crystal and stationary counter at beginning and end of scan, each for 25.0% of total scan time
Standard reflections	3 measured every 97 reflections
Theta range for data collections	3.65°–37.22°
Index ranges	$-1 \le h \le 8$, $-8 \le k \le 1$, $-15 \le l \le 15$
Reflections collected	1547
Independent reflections	378 [R_{int} = 0.0515]
Absorption correction	Indexed faces
Data/restraint/parameters	378/1/33
Goodness-of-fit	1.161
Final R-indices (all data)	$R1$ = 0.0283, $wR2$ = 0.0731
Absolute structure parameter	0.43(7)
Extinction coefficient	0.010(2)
Largest diff-peak and hole	0.429 and −0.588 eÅ^3

Note. $R1 = \sigma \|\|F_o| - |F_c|\|/\sigma|F_o|$, $wR2 = [\sigma[wF_o^2 - F_c^2]^2/\sigma[wF_o^2]^2]^{1/2}$; G.o.o.F = $\sigma\|\|F_o| - |F_c|\|/\sigma|F_o|$; $P = (\max F_o^2 + 2F_c^2)/3$, $w = 1/[\sigma^2F_o^2 + (0.0418P)^2 + 0.14P]$

$ScMnO_3$. Single crystals of $ScMnO_3$ were grown from a PbF_2 flux in a platinum crucible. The weights used were 5.99 g PbF_2, 0.51 g Sc_2O_3, and 1.00 g MnO. The temperature program involved heating to 1280° at 100°C/hr, soaking for 4 hr at this temperature, followed by cooling at 2°C/hr to 985°C. Black, highly reflective, thin (5 μm) plates of area 0.5 × 0.5 mm were formed. The flux was dissolved in warm HNO_3. EDAX analysis showed no detectable Pt or Pb in the crystals.

Magnetic Measurements

Magnetic data were collected on finely ground polycrystalline samples using a Quantum Design MPMS SQUID magnetometer at temperatures ranging from 5 to 300 K and applied fields ranging from 0.05 to 4.0 T. A scan length of 6 cm was used and 20 measurements were performed over the scan length. A total of three scans were averaged

TABLE 3

Observed Line Positions and Relative Intensities for Polycrystalline $InMoO_3$ from Guinier Powder X-Ray Data (a = 5.8758(4), c = 11.471598) Å)

hkl	*d* (Å)	I_{REL}	*hkl*	*d* (Å)	I_{REL}
002	5.7299	23	302	1.6266	5
102	3.8076	3	116	1.6024	36
110	2.9380	35	206	1.5285	2
004	2.8678	43	220	1.4685	5
111	2.8464	35	304	1.4598	40
112	2.6148	100	008	1.4337	5
104	2.4984	4	117	1.4315	8
113	2.3303	2	222	1.4232	18
114	2.0525	49	108	1.3801	4
204	1.9024	5	224	1.3072	8
115	1.8080	10	118	1.2889	8
106	1.7895	7	226	1.1651	12
300	1.6965	53			

for each data point. All data were corrected for the diamagnetic contribution of a Kel-F sample holder. Core diamagnetism corrections for the substituent elements were not applied. All samples were zero-field cooled and measured by heating unless otherwise noted.

Neutron Diffraction

Neutron powder diffraction patterns for $InMnO_3$ were collected at two constant wavelength sources, the McMaster Nuclear Reactor (λ = 1.3920 Å) and the DUALSPEC facility (λ = 2.5040 Å) at the AECL Chalk River laboratories. The McMaster facility has been described previously (11). The DUALSPEC diffractometer is based on a 800-element multidetector array. In both cases data were collected over a wide angular range in steps of 0.1° (2θ). The temperatures from 5 to 295 K were investigated using either a closed-cycle refrigerator or a liquid-helium cryostat in zero applied magnetic field.

X-Ray Powder Diffraction

Powder data were collected using a Guinier–Hägg camera, IRDAB XDC700, with Cu$K\alpha_1$ radiation and a silicon internal standard. Films were read using a computer-controlled, automated LS-20 line scanner (KEJ Instruments).

Single Crystal X-Ray Data for $ScMnO_3$

Details concerning the crystal and data collection procedures are given in Tables 1 and 2. Crystal dimensions were measured with the aid of a video camera. Refinement was carried out using the SHELXTL PC program on an 80486 personal computer.

RESULTS AND DISCUSSION

Crystal Structure

$InMnO_3$. Twenty-six reflections were observed on the Guinier film, 25 of which were consistent with a $LnMnO_3$ ($P6_3cm$) type cell with a = 5.8758(4) Å and c = 11.4715(8) Å. The other very weak reflection appeared to be due to

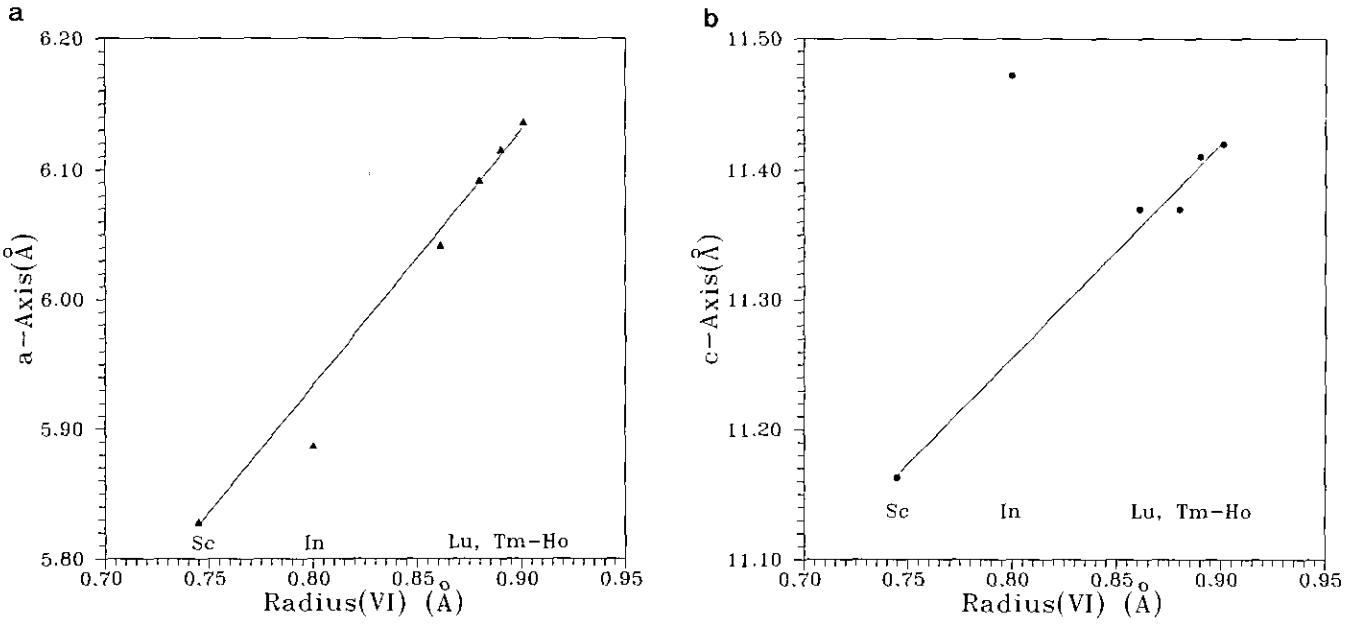

FIG. 1. Dependence of unit cell constants on ionic radii (VI) for R in the series $RMnO_3$ with the $LuMnO_3$ structure, R = Ho–Lu, In, and Sc: (a) a-axis and (b) c-axis.

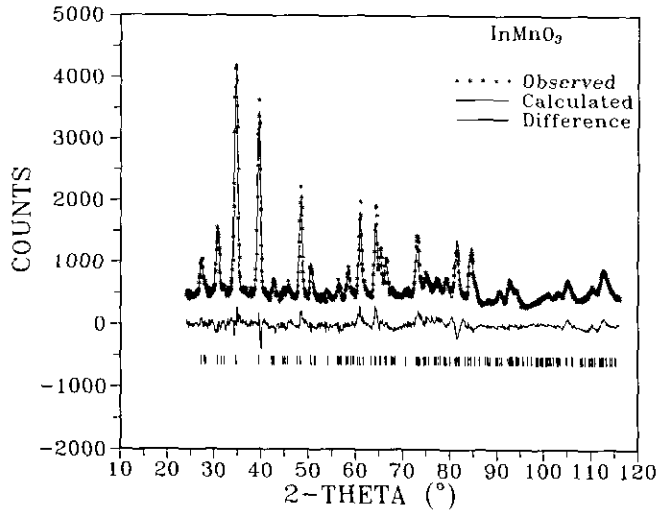

FIG. 2. Powder profile analysis of neutron powder diffraction data for $InMnO_3$.

In_2O_3, consistent with the excess of indium oxide used during the synthesis, as mentioned earlier. The observed line positions and relative intensities are shown in Table 3. Of these, the 18 strongest lines are also consistent with the smaller $YAlO_3$ ($P6_3/mmc$) cell. The remaining lines, although weak, clearly require the larger $P6_3cm$ cell.

It is of interest to compare the structural details for $InMnO_3$ with those of the isostructural series $RMnO_3$ where R = Ho, Er, Tm, Ln, Y, and Sc. The unit cell constants for these compounds as a function of the sixfold radius of the R(III) species are plotted in Figs. 1a and 1b. Note that the point for $InMnO_3$ deviates negatively by a small amount, 0.09 Å, for the a-axis cell constant and deviates positively by a huge amount, 0.22 Å, for the c-axis case. In fact, the c-axis for $InMnO_3$ is the largest for any $RMnO_3$ phase, exceeding even that for $HoMnO_3$ by 0.06 Å, in spite of the fact that the Ho(III) radius exceeds

TABLE 4
Neutron Powder Profile Refinement Results for $InMnO_3$

Space group	$P6_3cm$	No. parameters	23
a (Å)	5.8685(9)	Observed parameters	913
c (Å)	11.465(3)	Independent hkl	134
Lineshape	Gaussian	2θ range (°)	24–115
Step width (2θ)	0.10(°)	Temperature	295 K
R_P	0.071		
R_{WP}	0.091		
R_E	0.039		
S^a	2.34		
D–W^b	0.67		

Note. $R_{WP} = \{[\sum w(Y_{obs} - Y_{cal}/c)^2/\sum w\ Y_{obs}^2\}^{1/2}$; $R_P = \sum | Y_{obs} - Y_{cal}/c|/\sum Y_{obs}$; $R_E = [(N - P)/\sum w\ Y_{obs}^2]^{1/2}$.

[a] Square root of goodness-of-fit.

[b] Weighted Durbin–Watson statistic.

TABLE 5
Atomic and Thermal Parameters for $InMnO_3$

Atom	Position	x	y	z	B (Å^2)	U(eq) (Å^2)
In1	2a	0	0	0.2610(54)	3.68(1.24)	0.047(16)
In2	4b	1/3	2/3	0.2341(41)	1.35(50)	0.017(6)
Mn	6c	0.3214(53)	0	0	0.559(23)	0.007(3)
O1	6c	0.3012(23)	0	0.1545(27)	1.54(23)	0.019(3)
O2	6c	0.6538(24)	0	0.3247(26)	1.18(19)	0.015(2)
O3	2a	0	0	0.4713(35)	0.11(20)	0.001(2)
O4	4b	1/3	2/3	0.0085(33)	2.54(22)	0.032(3)

that of In(III) by about 10%. This suggests strongly that there are significant differences between the In–O and R–O bonding polyhedra. Such differences will be discussed in detail in a later section.

The results of a powder profile analysis of room temperature NMR neutron diffraction data are shown in Fig. 2 and Tables 4 and 5. Refinement was carried out with the software package DBWS 9006PC and an IBM-compatible 80486 personal computer. Although the refinement converged to the parameters listed in Table 5, the residuals were somewhat greater than those normally obtained with data from this source, yet the ratio, $R_{WP}/R_E = 2.3$, is acceptable. It is fair to say from this analysis that the $P6_3cm$ model is a reasonable description of the structure of $InMnO_3$.

$ScMnO_3$. Refinement was carried out in $P6_3cm$, No. 185, as for $InMnO_3$ and $LuMnO_3$. Tests were also done in the centric group $P6_3/mcm$, No. 193, and the lower

TABLE 6a[2]
Atomic Coordinates and Equivalent Isotropic Displacement Parameters for $ScMnO_3$

	x	y	z	U(eq) (Å^2)
Sc(1)	0	0	0.2738(2)	0.004(1)
Sc(2)	1/3	2/3	0.2312(2)	0.005(1)
Mn	0.3335(1)	0	0(2)	0.005(1)
O(1)	0.3031(6)	0	0.1683(9)	0.007(1)
O(2)	0.6358(6)	0	0.3328(9)	0.006(1)
O(3)	0	0	0.4675(14)	0.007(2)
O(4)	1/3	2/3	0.0240(11)	0.007(1)

Note. U(eq) is defined as one third of the trace of orthogonalized U_{ij} tensor.

[2] See NAPS document No. 05162 for 01 pages of supplementary material. Order from ASIS/NAPS, Microfiche Publications P. O. Box 3513, Grand Central Station, New York, NY 10163. Remit in advance $4.00 for microfiche copy or for photocopy, $7.75 up to 20 pages plus $.30 for each additional page. All orders must be prepaid. Institutions and Organizations may order by purchase order. However, there is a billing and handling charge for this service of $15. Foreign orders add $4.50 for postage and handling, for the first 20 pages, and $1.00 for additional 10 pages of materials, $1.50 for postage of any microfiche orders.

symmetry group, $P3c1$, No. 158. In both cases the results were less satisfactory than those for $P6_3cm$, with significantly larger residuals and larger features in the difference map.

In the course of refinement in $P6_3cm$ there arose an indication of racemic twinning. Such a parameter was included, and final values indicated approximately equal contributions from both right- and left-handed components.

The results of the single-crystal structure analysis of $ScMnO_3$ are shown in Tables 6a and 6b. The residuals, Table 2, are reasonable and the esd's are smaller than for the neutron powder solution for $InMnO_3$. No esd's were reported in the earlier X-ray single crystal solution for $LuMnO_3$ (4). Thermal ellipsoids for 01 and 02 are flattened significantly along the c-axis, but this may reflect the exceedingly small crystal thickness and attendant difficulties in correcting accurately for absorption.

Comparison: $InMnO_3$ with $ScMnO_3$ and $LuMnO_3$

Selected bond distances and angles are shown in Tables 7a and 7b for all three isostructural compounds. The coordination polyhedra about Mn, $R1$, and $R2$ are shown in Fig. 3. The Mn–O polyhedron is a distorted trigonal bipyramid and both the $R1$–0 and $R2$–0 polyhedra are monocapped octahedra. Note that the average Mn–O distance is essentially constant for the three materials and in good accord with the sum of ionic radii. For $R1$–0 and $R2$–0 the octahedron is formed by the bonds to O1 and O2 and the average $R1$–O1,O2 and $R2$–O1,O2 distances are in good agreement with the sum of the radii. The capping oxygens are O3 and O4 and the $R1$–O3 and $R2$–O4 distances are slightly larger than, but in most cases still within, 0.1 Å of the sum of the radii for $ScMnO_3$ and $LuMnO_3$. For $InMnO_3$ in contrast, the In1–O3 and In2–O4 distances are 0.20 and 0.37 Å greater than the sum of the radii. This, of course, results from the greatly increased c-axis for $InMnO_3$ and suggests that the capping atom is more weakly bonded to the octahedron in this case; i.e., the In–O coordination number is approaching 6 rather than 8 as found for yttrium in the $YAlO_3$ structure or 7 for Sc and Lu as in $ScMnO_3$ and $LuMnO_3$, respectively. These longer In–O3 and In–O4 bonds have implications for interlayer Mn–Mn superexchange, as discussed later. These differences may be traceable to the distinct electronic structure of In^{3+} which has filled d-orbitals, in contrast to Sc^{3+} and Lu^{3+} with empty d-orbitals.

TABLE 6b
Anisotropic Displacement Parameters (Å^2) for $ScMnO_3$

	$U11$	$U22$	$U33$	$U23$	$U12$
Sc(1)	0.005(1)	0.005(1)	0.003(1)	0	0.002(1)
Sc(2)	0.005(1)	0.005(1)	0.005(1)	0	0.003(1)
Mn	0.007(1)	0.007(1)	0.002(1)	0.000(1)	0.004(1)
O(1)	0.007(1)	0.011(1)	0.002(2)	0.003(2)	0.006(1)
O(2)	0.008(1)	0.009(1)	0.001(2)	0.001(2)	0.005(1)
O(3)	0.008(1)	0.008(1)	0.005(5)	0	0.004(1)
O(4)	0.006(1)	0.006(1)	0.007(3)	0	0.003(1)

Note. The anisotropic displacement factor exponent takes the form $-2\pi^2\,[h^2a^{*2}U11 + \cdots + 2hka^*b^*U12]$.

TABLE 7a
Selected Bond Distances for $ScMnO_3$, $InMnO_3$, and $LuMnO_3$ (6)

	$ScMnO_3$ (Å)	$InMnO_3$ (Å)	$LuMnO_3$ (Å)
Mn–O1	1.877(10)	1.775(2)	1.84
Mn–O2	1.889(10)	2.02(3)	1.93
Mn–O3	1.977(3)	1.91(3)	2.06
Mn–O4(×2)	1.961(2)	1.99(2)	1.98
⟨Mn–O⟩	1.93	1.94	1.95
Σ Radii	1.96	1.96	1.96
$R1$–O1(×3)	2.124(7)	2.15(4)	2.18
$R1$–O2(×3)	2.223(4)	2.16(4)	2.35
$R1$–O3	2.16(2)	2.41(7)	2.42
$R2$–O1(×3)	2.155(4)	2.25(2)	2.19
$R2$–O2(×3)	2.179(6)	2.18(3)	2.31
$R2$–O4	2.31(1)	2.59(6)	2.36
⟨$R1$–O1,O2⟩	2.17	2.16	2.27
⟨$R2$–O1,O2⟩	2.17	2.22	2.25
Σ Radii	2.17	2.22	2.28

TABLE 7b
Selected Bond Angles (°) for $ScMnO_3$, $InMnO_3$, and $LuMnO_3$

	$ScMnO_3$	$InMnO_3$	$LuMnO_3$
O1–Mn–O2	179.9(2)	179.7(2)	174.0
O1–Mn–O3	95.2(5)	96.1(2)	93.0
O4–Mn–O4	118.2(2)	116.3(2)	115.5
O2–Mn–O4	95.1(1)	90.6(1)	91.4
O3–Mn–O4	120.78(3)	121.7(8)	122.1
O2–Mn–O3	84.9(5)	90(2)	93
O1–Mn–O4	84.8(4)	84(1)	85
Mn–O3–Mn	116.7(3)	117(2)	119.1
Mn–O4–Mn	118.2(2)	119.8(3)	118.9
O1–$R1$–O1	92.2(4)	91(2)	95
O1–$R1$–O2	163.6(5)	165(3)	168
O1–$R1$–O2	76.6(1)	79(1)	77
O2–$R1$–O2	111.6(3)	109(2)	109
O1–$R1$–O3	123.7(3)	125(1)	122
O2–$R1$–O3	72.7(3)	70(2)	71
O1–$R2$–O1	109.9(3)	105(2)	112
O1–$R2$–O2	76.9(2)	76(1)	78
O1–$R2$–O2	167.6(5)	175(2)	163
O2–$R2$–O2	95.3(3)	99(2)	92
O2–$R2$–O4	121.4(2)	124.7(8)	123
O1–$R2$–O4	71.0(3)	71(1)	73
$R1$–O1–Mn	129.1(3)	129(2)	124
$R2$–O2–Mn	123.6(3)	120(1)	127

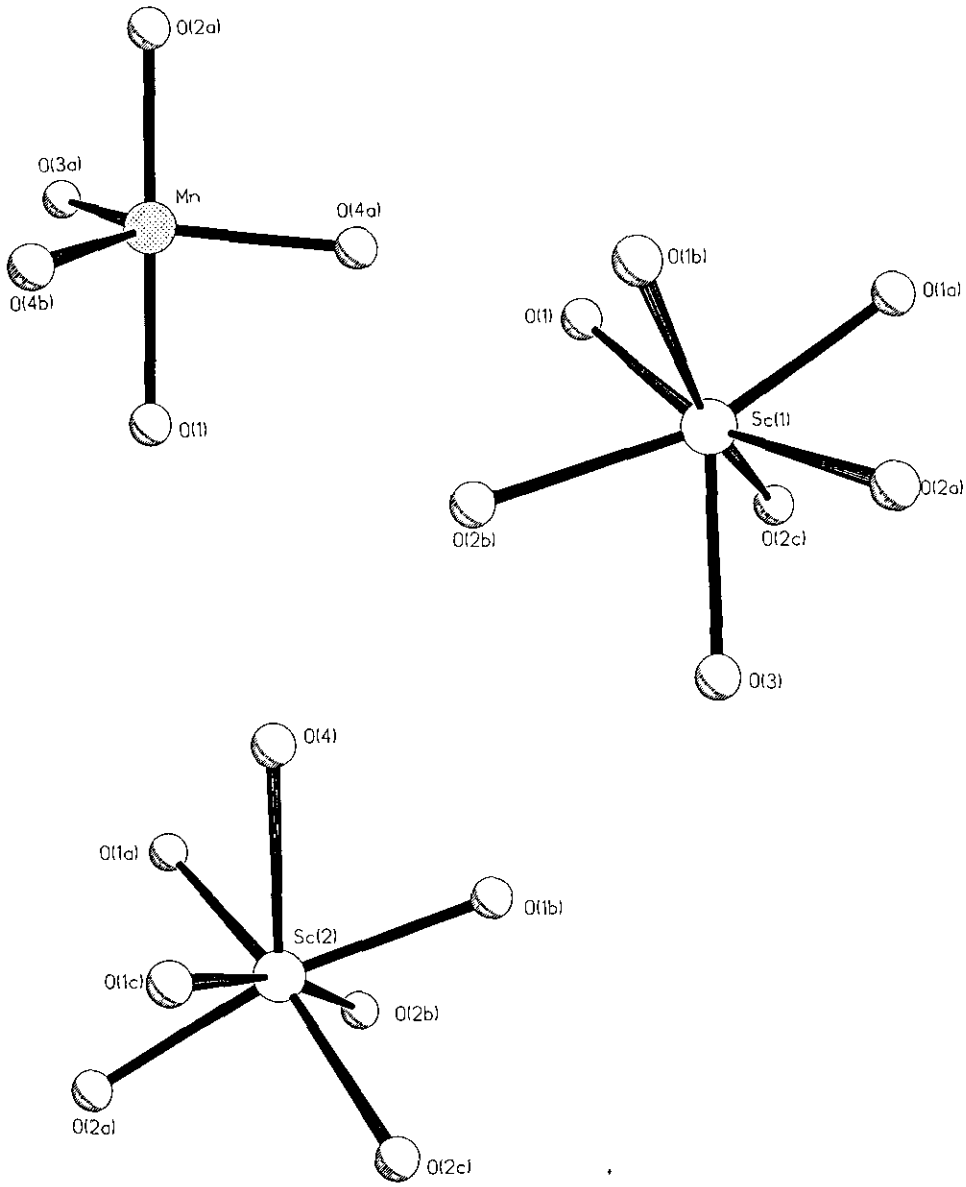

FIG. 3. Coordination polyhedra for Mn–O and Sc–O in the $P6_3cm$ ($LuMnO_3$) structure type.

It is also important to note that this indium anomaly appears to be a general phenomenon in isostructural series involving the rare earths and indium. For example, $InCrO_3$ exists as a high pressure polymorph with the *Pmna* $GdFeO_3$ structure which is the stable form of the $RCrO_3$ series where R is a rare earth (12, 13). Figure 4 shows a plot of cell volume versus ionic radius for the small R members of the series plus In and the anomaly is clearly seen. Parallel results exist for the $RGaO_3$ compounds (14–16). In fact, sixfold coordination is found for In in $InGaO_3$ which is reported to form in the $P6_3/mmc$, $YAlO_3$ structure (16).

Figure 5 shows a polyhedral representation of the $P6_3cm$ or $LuMnO_3$ structure type in which it can be seen that layers of corner-sharing Mn–O trigonal bipyramids are separated by layers of edge-sharing R–O octahedral. As mentioned, the $P6_3cm$ structure is a slight distortion of the $YAlO_3$ type, $P6_3/mmc$. The latter can be described as a stuffed delafossite ABO_2 structure (17) in which an extra oxygen has been inserted into the plane occupied by the A-atoms which are linearly coordinated in delafossite and are thus transformed to trigonal bipyramidal sites in $YAlO_3$. The stacking of the layers involving the magnetic atoms is ABCABC in delafossite. Alternatively, the $LuMnO_3$ structure can be re-

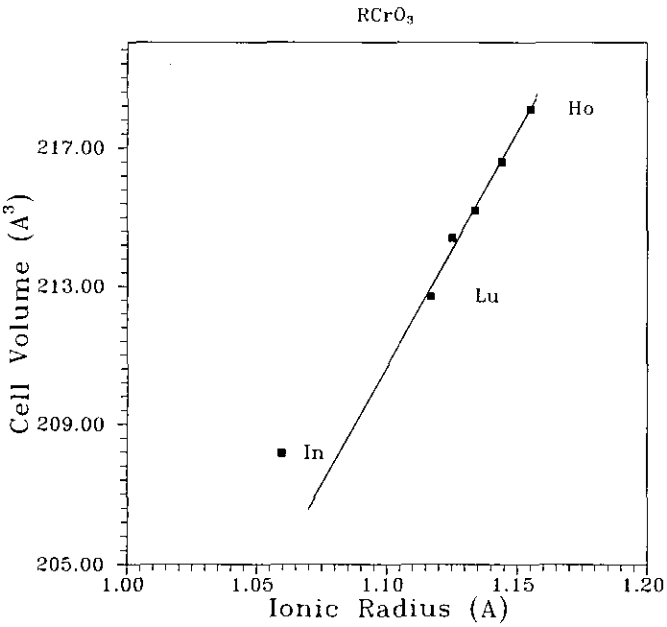

FIG. 4. Dependence of unit cell volume on ionic radii of the $RCrO_3$ series [$GdFeO_3$] with R = Ho–Lu and In.

lated to the CdI_2 type in which the empty sites in van der gap are filled by a Mn–O hexagonal net. These nets are stacked in an ABAB pattern, a significant difference from delafossite, in the $LuMnO_3$ structure.

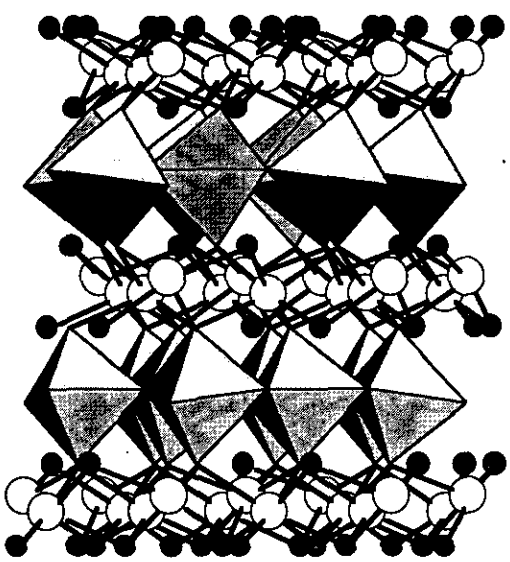

FIG. 5. The $P6_3cm$ structure of $InMnO_3$ as determined by polycrystalline neutron diffraction. Indium is represented as large open circles, manganese is located at the center of the distorted polyhedra, and oxygen is represented as small filled circles and is also located at the apices of all polyhedra.

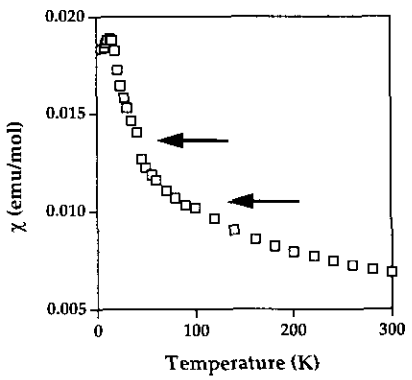

FIG. 6. Magnetic susceptibility data for $InMnO_3$ at an applied field of 0.05 T.

Magnetic Susceptibility

Susceptibility data for the range 4.5 to 300 K are shown in Fig. 6 for a low applied field of 0.05 T. There are clearly two anomalies or discontinuities at 120 K, and about 40 K, and a weak maximum at 15 K. The inverse susceptibility, see Fig. 7, indicates non-Curie–Weiss behavior over most of the range. A possible linear region exists above 225 K, which yields $\theta = -430$ K, an indication of strong antiferromagnetic correlations, but data at much higher temperatures are needed to characterize the paramagnetic regime.

Figures 8a–8d show the marked dependence of the low temperature susceptibility on the applied magnetic field. Both low temperature anomalies at 40 and 15 K disappear with an increase in the applied field. The 40 K inflection is gone by 0.2 T and the 15 K maximum becomes an inflection. The latter feature is removed completely at 0.40 T.

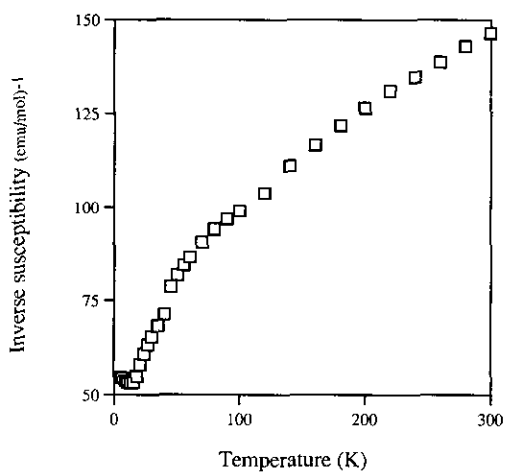

FIG. 7. Inverse magnetic susceptibility data for $InMnO_3$ showing nonlinear behavior for the temperature range studied.

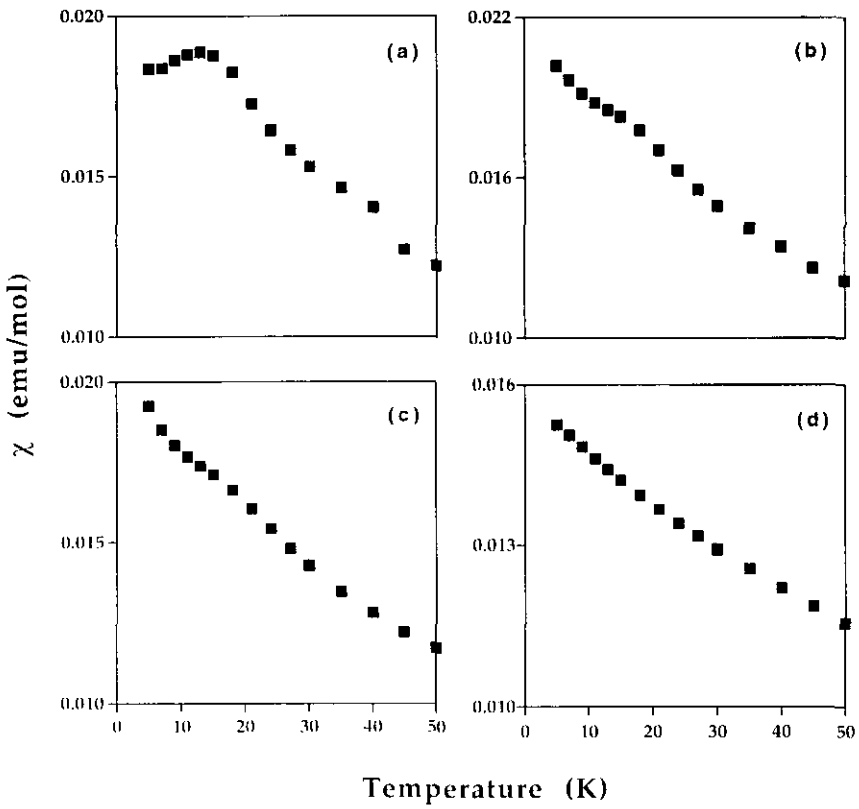

FIG. 8. Dependence of the magnetic susceptibility of $InMnO_3$ at low temperatures for various values of the applied field: (a) 0.05 T, (b) 0.25 T, (c) 0.5 T, and (d) 4.0 T.

Magnetic Neutron Diffraction

Figure 9 displays the neutron diffraction pattern at 4.5 K obtained under high resolution conditions on DUALSPEC (λ = 2.5040 Å). Eight new reflections appear at this temperature which were not present at 200 K. Seven of these can be indexed as (h 0 l/2) or (h 1 l/2), where the indices refer to the chemical cell and h = 1 or 2. If these are all magnetic reflections, this requires, clearly, a doubling of the chemical cell c-axis in the magnetic unit cell or a propagation vector of $\bar{\mathbf{q}} = (00\frac{1}{2})$. This is in sharp contrast to the case of $YMnO_3$, where the magnetic reflections are of the type (h 0 l), h = 1 or 2, and the magnetic and chemical cells are identical in size, i.e., $\bar{\mathbf{q}} = (000)$ (7).

In an attempt to extract relative intensities, each magnetic reflection was fitted to a Gaussian line shape. At this point it was discovered that none of the reflections

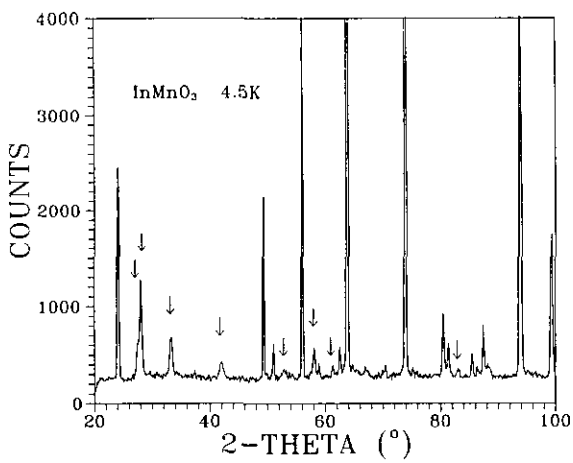

FIG. 9. Neutron diffraction pattern for $InMnO_3$ at 4.5 K obtained at the DUALSPEC source. λ = 2.5040 Å. Magnetic reflections are identified.

TABLE 8

Magnetic Reflections (h 0 l/2) or (h1 l/2) for $InMnO_3$ at 4.2 K

$h\ k\ l$	2θ	I_{MAG}	FWHM (obs) (°)	FWHM (Res. limit) (°)
1 0 ½	29.04	172(9)	0.39(1)	0.28
1 0 ⅜	34.84	218(8)	0.54(2)	0.27
1 0 ⅝	42.90	116(9)	0.72(8)	0.23
1 0 ⅞	53.80	77(10)	0.71(12)	0.23
2 0 ½	59.06	102(17)	0.33(1)	0.22
2 0 ⅜	62.20	72(6)	0.29(5)	0.24
2 1 ⅜	83.92	83(12)	0.54(5)	0.31

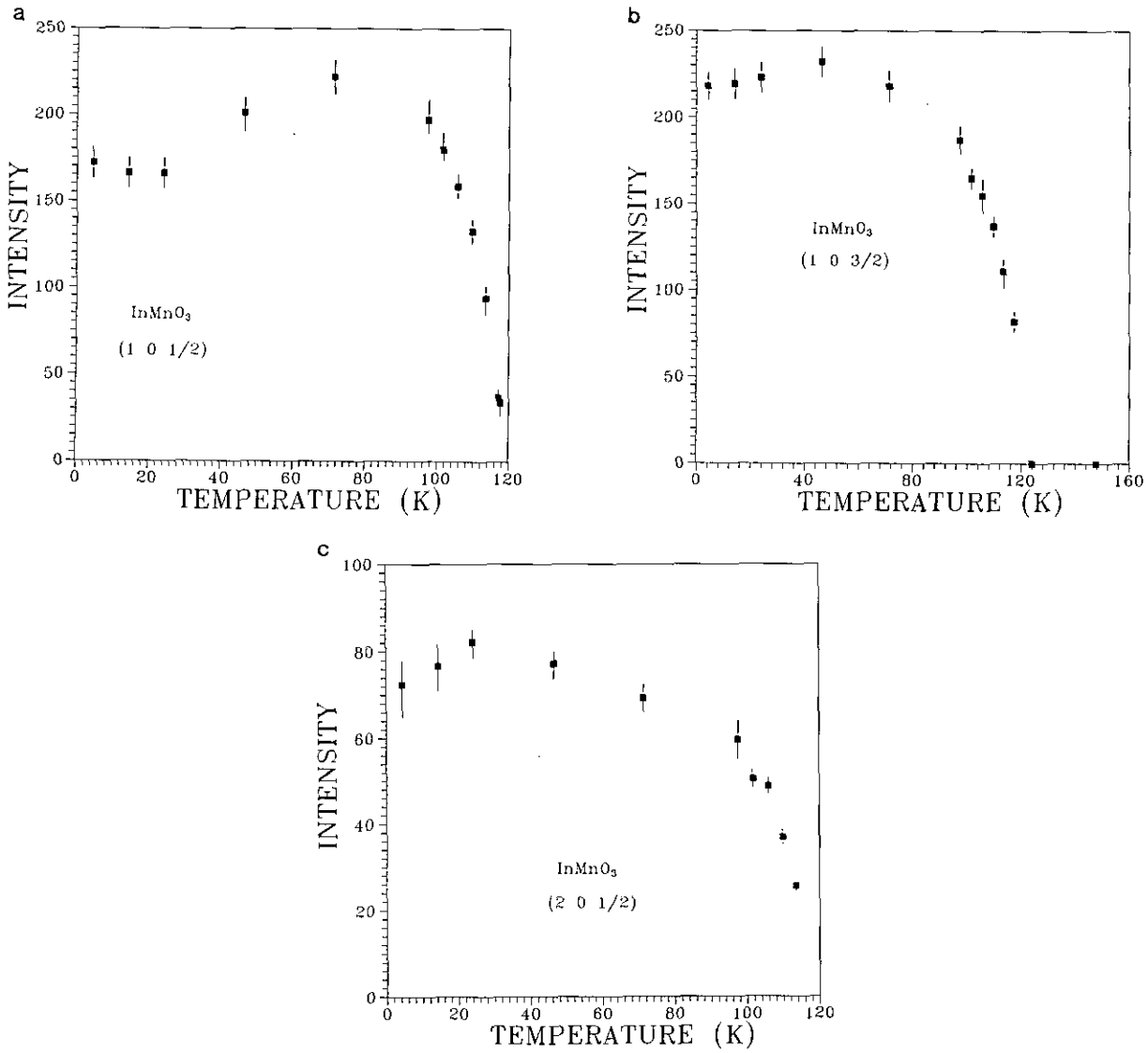

FIG. 10. Temperature dependence of the intensity for three selected magnetic reflections of $InMnO_3$. (a) (1 0 $\frac{1}{2}$); (b) (1 0 $\frac{3}{2}$); (c) (2 0 $\frac{1}{2}$).

in this class were truly resolution limited as can be seen in Table 8: Note that the peak width increases with the index l for the best defined series, (1 0 l/2).

Figures 10a, 10b, and 10c show the temperature dependence of three selected reflections (1 0 $\frac{1}{2}$), (1 0 $\frac{3}{2}$), and (2 0 $\frac{1}{2}$). First, note that all three indicate an ordering temperature near 120 K. This is a significantly higher temperature than that found for the lanthanide series, $LuMnO_3$–$HoMnO_3$, where true T_c's range from 76 K (Ho) to 91 K (Lu) (8), but essentially the same as that reported for $ScMnO_3$ (8), although detailed studies of this latter material are not available. Thus, the susceptibility anomaly at 120 K for $InMnO_3$ can be assigned to the onset of interlayer spin correlations which remain finite in size down to the lowest temperatures studied here. Note also the unusual shape of the curves in Figs. 10a–10c in that a maximum appears at somewhat different temperatures depending on the reflection indices. This indicates a spin reorientation among the finite range interplanar coupled spins and this may be associated with the susceptibility anomalies near 40 and 15 K which disappear upon increase of the applied magnetic field.

Close examination of the (1 0 $\frac{1}{2}$) reflection, Fig. 11, shows clearly the presence of a second, overlapping reflection. Attempts to fit this region to two Gaussians gave not unreasonable results, but the FWHM was particularly large, 0.96(3)°, which is about four times the resolution limited value. This broad, low angle reflection can be indexed as (1 0 0) indicating that it arises from short range intraplanar spin correlations. (1 0 0) is a prominent

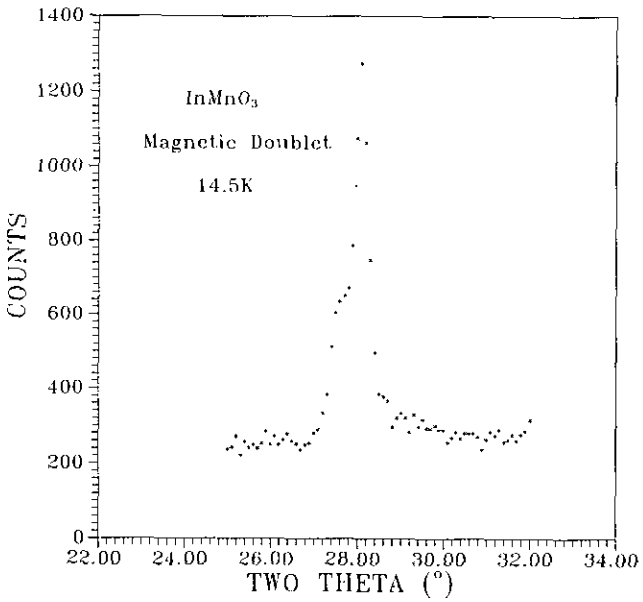

FIG. 11. The (1 0 0), (1 0 $\frac{1}{2}$) magnetic doublet.

magnetic reflection for the $LnMnO_3$ compounds and suggests a triangular type structure.

Examination of the (1 0 0) feature at higher temperatures indicates that the lineshape is not Gaussian but instead is close to the classic Warren lineshape. This lineshape is manifest in polycrystalline diffraction data from samples which are two-dimensional such as various forms of disordered graphites or polycrystalline surface layers. Warren showed that the scattered power from such a system is given by

$$P_{2\theta} = Km \frac{F_{hk}^2(1 + \cos^2 2\theta)}{2(\sin\theta)^{3/2}} \frac{(L)_{1/2}}{\pi\lambda} F(a), \qquad [1]$$

where $a = (2\sqrt{\pi}\, L/\lambda)(\sin\theta - \sin\theta_0)$, K is a constant, m is the multiplicity, F_{hk} is the two dimensional structure factor, λ is the wavelength, L is a two-dimensional correlation length, and θ_0 is the peak position (18). The function $F(a)$ is tabulated. Although it is not immediately obvious from the above, the Warren lineshape features a sharp rise in scattered intensity for $\theta < \theta_0$ followed by a much more gradual decrease for $\theta > \theta_0$.

The applicability of the Warren lineshape analysis for the (1 0 0) or, more correctly, the (10) reflection for $InMnO_3$ is best seen for temperatures at 120 K or above where the (1 0 $\frac{1}{2}$) reflection has vanished, Figs. 12a and 12b for both high and low resolution data. In Fig. 12b, the low angle Gaussian is the (0 0 2) Bragg reflection. Extraordinarily, the broad (1 0) feature persists up to room temperature as is apparent from Fig. 13. For lower temperatures the (1 0 0)/(1 0 $\frac{1}{2}$) doublet was fitted with a convolution of a Warren and a Gaussian lineshape function which gave in all cases excellent results comparable to or superior to that for a two Gaussian fit as judged by the reduced chi-squared values. Examples of some low temperature fits are shown in Fig. 14.

The implication of the above result is that the intraplanar magnetic correlations in $InMnO_3$, which are measured by the (1 0) reflection, are rigorously two-dimensional over the entire temperature range studied. From Eq. [1] it is clear that one can extract a two-dimensional correlation length, L, from the fits and the temperature dependence of L is displayed in Fig. 15. L rises slowly from a room

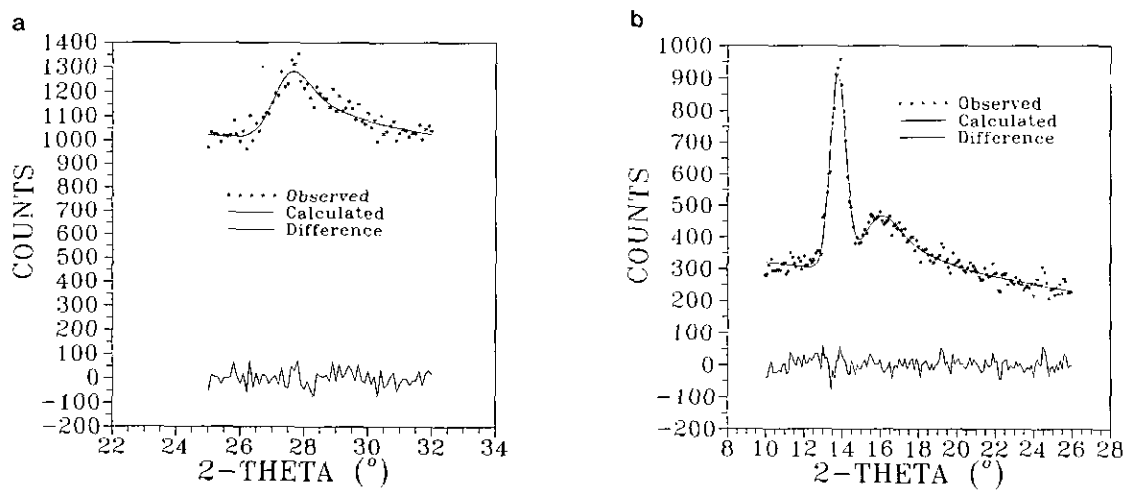

FIG. 12. The (1 0 0) or (1 0) reflection for $InMnO_3$. The solid line is a fit to the Warren lineshape equation [1]. (a) High Resolution DUALSPEC data, T = 123 K; (b) lower resolution MNR data, T = 120 K. The reflection at lower angles is (0 0 2).

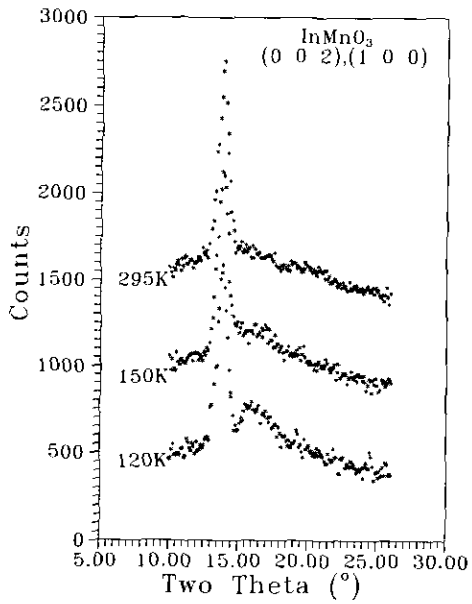

FIG. 13. Persistence of the broad (1 0) reflection for $InMnO_3$ up to 295 K.

temperature value of 3.6(7) Å, which is essentially a nearest neighbor distance, with decreasing temperature until near 120 K where it increases rapidly reaching maximum values near 50 Å at the lowest temperatures. Thus, the sharp increase of the range of the two-dimensional magnetic correlations appears to be coupled to the onset of short-range interplanar correlations which occurs over the same temperature range.

This basic result for $InMnO_3$, that no true long-range magnetic intraplanar or interplanar order exists, is in sharp contrast to the situation for $LuMnO_3$ and $ScMnO_3$. Both of these materials show true long-range order (LRO) below temperatures of 91 K (Lu) and 127 K (Sc) with a magnetic structure described by a propagation vector $\mathbf{q} = (000)$, that is, chemical and magnetic cells of the same size. The intraplanar spin configuration in this magnetic structure is the so-called triangular type in which the spins on the corners of the edge-sharing equilateral triangles comprising the hexagonal net are oriented at 120° to each other. Such a magnetic structure occurs due to frustration

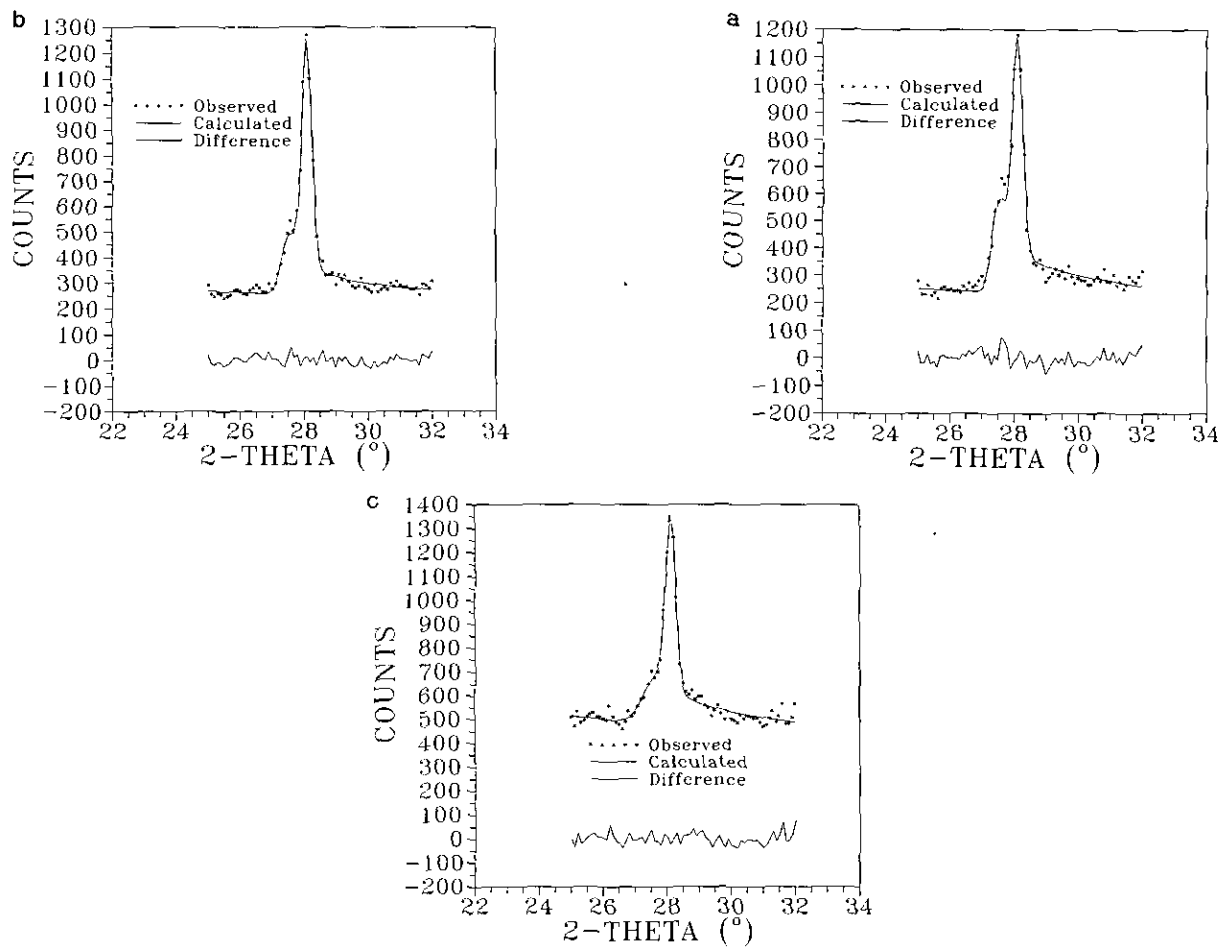

FIG. 14. Fits of the (1 0)/(1 0 ½) magnetic doublet to a convolution of Warren and Gaussian line shapes for selected temperatures: (a) 14.5 K, (b) 71.6 K, and (c) 109.8 K.

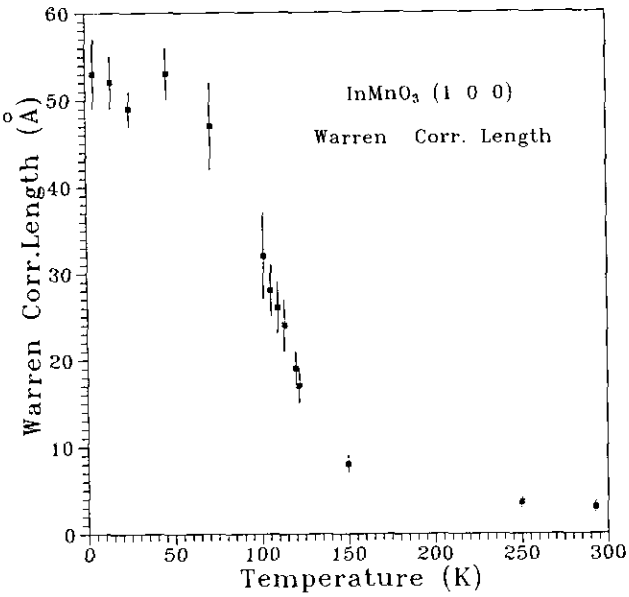

FIG. 15. Temperature dependence of L, the two-dimensional Warren correlation length (Å) for $InMnO_3$ from the (1 0) reflection.

between nearest neighbor spins which arises when the exchange coupling is antiferromagnetic.

For the $LuMnO_3$ structure type there exist two magnetic layers per chemical cell with the atoms in each layer displaced form those in adjacent layers by the hcp translation vector $(\frac{1}{3}\frac{2}{3}\frac{1}{2})$ thus, the inherent intraplanar frustration is compounded by the ABAB stacking of the layers. For $LuMnO_3$ and $ScMnO_3$ the stacking of the triangularly spin-coupled layers is such that the chemical cell periodicity is retained (7, 8).

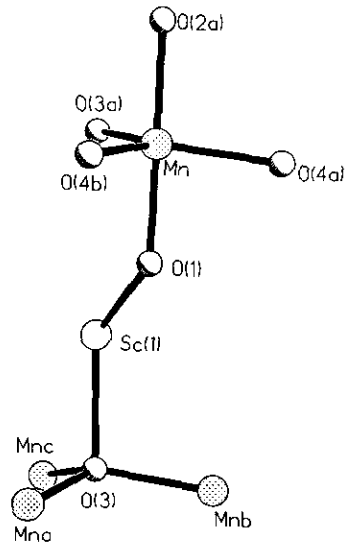

FIG. 16. An interplanar superexchange pathway in $RMnO_3$.

As LRO is not possible in only two dimensions for any triangular lattice, a necessary condition for its observation is a finite interplanar exchange coupling. In the $LuMnO_3$ structure type, interplanar exchange, which will be significantly weaker than intraplanar coupling, involves two superexchange pathways, Mn–*O*1–*R*1–03–Mn and Mn–O2–R2–04–Mn, one of which is shown in Fig. 16. It has been pointed out already, that in $InMnO_3$ the In1–03 and In2–04 distances are anomalously long relative to the corresponding Sc–O and Lu–O distances. As the superexchange interaction depends strongly on orbital overlap integrals which are in turn a strong function of interatomic distance, one expects a significantly weaker interplanar exchange in $InMnO_3$ than $LuMnO_3$ or $ScMnO_3$. Thus, there may be a clearly identifiable structural origin to the absence of LRO in $InMnO_3$.

These results for $InMnO_3$ can be discussed in the context of available theory for the type of magnetic sublattice present and compared to those reported recently for structurally similar phases. As mentioned earlier the ABAB pattern for the magnetic atom layers in $InMnO_3$ is an uncommon stacking sequence for magnetic insulators as most other well-studied examples have either simple hexagonal stacking, AAA, such as in NiAs structure compounds, or the salts $CsMnBr_3$ and $RbMnBr_3$, or rhombohedral stacking, ABCABC, examples being delafossite structure materials, $CuCrO_2$, $CuFeO_2$, and others and ordered NaCl structure oxides $LiNiO_2$, $LiCrO_2$ etc.

Reimers and Dahn (6) have carried out an analysis of possible LRO in all three stacked hexagonal lattices within the context of mean-field theory and considering three exchange interactions, J_1 and J_2, nearest and next-nearest neighbor intraplanar, respectively, and J_3, the interplanar coupling. Their results for ABAB stacking show that an interesting region of the phase diagram occurs for $J_2/|J_1| \sim 0$ and $J_3/|J_1| \sim 0$ which is likely to be appropriate to the three materials in question. For $J_3 = 0$ no LRO is found, consistent with all previous work, and short range triangular intraplanar ordering is predicted. For finite $J_3/|J_1|$ and $J_2/|J_1| = 0$ a large ground state degeneracy is also found which leads to predictions of only short-range order in the mean field limit. For small excursions from this region LRO is predicted but with incommensurate propagation vectors $(q, q, 0)$. However, as $J_3 \to 0$, $q \to \frac{1}{3}$. In the treatment of Reimers and Dahn the triangular structure is described by $\mathbf{q} = (\frac{1}{3}\frac{1}{3}0)$ as they treat only the two atom hcp lattice. For the $P6_3cm$, $LuMnO_3$ structure six atoms are involved, i.e., three times the volume, so the propagation vector for the triangular structure is $\mathbf{q} = (0\,0\,0)$. Thus, the Reimers and Dahn analysis is consistent, qualitatively, with our observations on the series $RMnO_3$ in that LRO is vulnerable to a vanishing J_3 and that a triangular magnetic structure is expected for small but finite $J_3/|J_1|$. Theoretical studies beyond the mean field approximation would

be welcome here to further clarify the situations as would experimental results for other ABAB stacked lattices.

It is worth noting that behavior parallel to that of $InMnO_3$ has been seen in other stacked triangular lattice systems with ABCABC rather than ABAB stacking. The mean field phase diagrams for ABAB and ABCABC stacking show some qualitative similarities (6). The ordered rock-salt oxide $LiNiO_2$ has been shown to exhibit spin-glass-like behavior with no long-range order (19). This has been attributed in part to very slight nonstoichiometry and Li/Ni intersite mixing, the inherent frustration and perhaps, the quantum, $S = \frac{1}{2}$ spin condition. The delafossite oxide $CuCrO_2$ exhibits magnetic Bragg peaks consistent with $\bar{\mathbf{q}} = (\frac{1}{3}\ \frac{1}{3}\ l)$, but these are broader that the resolution limit as for $InMnO_3$. The in-plane correlations in $CuCrO_2$ are of longer range than those for $InMnO_3$ which are essentially two-dimensional in nature. Another delafossite, $AgCuO_2$, also shows no long-range order with broad magnetic Bragg peaks consistent with a short-range incommensurate structure characterized by a wave vector (0.327, 0.327, 0) (21).

ACKNOWLEDGMENTS

We thank Mr. W. Gong for obtaining and interpreting the Guinier X-ray data, Dr. Guo Liu for computer software development, and R. Donaberger and Dr. I. Swainson for considerable assistance with the neutron experiments at DUALSPEC. J.E.G. acknowledges the Natural Science and Engineering Research Council of Canada for direct support via a Research Grant and for Infrastructure support for DUALSPEC. We thank McMaster University for direct support of the McMaster Nuclear Reactor. H.z.L. and D.M.G. acknowledge financial support under Grant DMR9022933 administered through the MIT Center for Materials Science and Engineering.

REFERENCES

1. D. M. Giaquinta and H.-C. zur Loye, *J. Am. Chem. Soc.* **114** 10,952 (1992); D. M. Giaquinta and H.-C. zur Loye, *Chem. Nat.* **6,** 365 (1994).
2. N. Kimizuka and T. Mohri, *J. Solid State Chem.* **78,** 98 (1989).
3. R. D. Shannon, *Acta Crystallogr. Sect. A* **32,** 751 (1976).
4. H. L. Yakel, W. C. Koehler, E. F. Bertaut, and E. F. Forrat, *Acta Crystallogr.* **16,** 957 (1963).
5. R. Norrestam, *Acta Chem. Scand.* **19,** 1009 (1965).
6. J. N. Reimers and J. R. Dahn, *J. Phys. Condens. Matter* **4,** 8105 (1992).
7. E. F. Bertaut and M. Mercier, *Phys. Lett.* **5,** 27 (1963).
8. W. C. Koehler, H. L. Yakel, E. O. Wollan, and J. W. Cable, *Phys. Lett.* **9,** 93 (1964).
9. D. M. Giaquinta, Ph.D. Thesis, Massachusetts Institute of Technology, Cambridge, MA, 1994.
10. B. M. Wanklyn, *J. Mater. Sci.* **7,** 813 and 821 (1972).
11. J. N. Reimers, J. E. Greedan, and M. Sato, *J. Solid State Chem.* **72,** 390 (1988).
12. S. Quezel-Ambrunaz and M. Mareschal. *Bull Soc. Fr. Mineral. Cristallogr.* **86,** 204 (1963).
13. R. D. Shannon, *Inorg. Chem.* **6,** 1474 (1967).
14. M. Marezio, J. P. Remeika, and P. D. Dernier, *Inorg. Chem.* **7,** 1337 (1968).
15. M. Marezio, J. P. Remeika, and P. D. Dernier, *Mater. Res. Bull.* **1,** 247 (1966); M. Marezio, *Trans. Am. Crystallogr. Assoc.* **5,** 29 (1969).
16. R. D. Shannon, C. T. Prewitt, *J. Inorg. Nucl. Chem.* **30,** 1389 (1968).
17. C. T. Prewitt, R. D. Shannon, and D. B. Rogers *Inorg. Chem.* **10,** 719 (1971).
18. B. E. Warren, *Phys. Rev.* **59,** 693 (1941).
19. J. N. Reimers, J. R. Dahn, J. E. Greedan, C. V. Stager, G. Liu, I. Davidson, and U. von Sachen, *J. Solid State Chem.* **102,** 542 (1993).
20. H. Kadowaki, H. Kikuchi and Y. Ajiro, *J. Phys. Condens. Matter* **2,** 4485 (1990).
21. Y. Oohara, S. Mitsuda, H. Yosizawa, N. Yaguchi, H. Kurizamam, T. Kurizama, T. Asano, and M. Mekata, Technical Report ISSP, Univ. of Tokyo, Ser A., No. 2714, 1993.